International Journal of Aerospace and Lightweight Structures
Vol. 3, No. 4 (2013) 487–502

DOI: 10.3850/S201042861400004X

STUDY ON THE QUASI-STATIC INDENTATION BEHAVIOR OF AL FOAM

Xinzhu Wang[1,2]*, Xianghe Peng[1] and Shan Tang[1]

[1] *Chongqing Key Laboratory of Heterogeneous Material Mechanics, Department of Engineering Mechanics, Postdoctoral Station of Mechanics, Chongqing University, Chongqing 400040, China.*

[2] *State Key Laboratory of Advanced Design and Manufacture for Vehicle Body, Hunan University, Changsha 410082, China.*

The response of closed-cell Al foams under the flat-end cylindrical indenter is experimentally and numerically investigated. The effects of the indenter diameter and the relative density of Al foam on the tearing energy, indentation hardness, energy absorbing capability and efficiency are also investigated. Experimental results show that the indentation load-displacement response obtained with the flat-end cylindrical indenter is similar to that under uniaxial compression. Cross-sectional views of the indented specimens show that the deformation is non-uniform and confined only to the region directly under the indenter with insignificant lateral extension. The tearing energy and the efficiency energy absorption of Al foam are independent of the indenter diameter and the relative density of Al foam. The indentation hardness decreases linearly with increasing of indenter diameter or decreasing of relative density, but the energy absorption capability increases linearly with the increase of indenter diameter and relative density. In order to study the effects of boundary condition, both rigid and simply supported boundary conditions are considered. At a certain range of indentation depth, the difference between the result with rigid foundation and that with simply supported condition is negligible. Results obtained with finite element simulation and experiments are found to be in satisfactory agreement.

Keywords: Al foam, Indentation, Tearing energy, Energy absorption.

1. Introduction

Metal foam has many advantages, such as relatively high ratio of stiffness to density, excellent noise absorption and vibration suppression, and easy recycle [Gibson and Ashby, 1997; Ashby *et al.*, 2000]. Therefore, it is of great potential for it to be used in lightweight or energy absorption structural components, and it has been receiving increasing attention in recent decades.

The low impact (or indentation) behavior of metal foam has been extensively investigated in recent years and much progress has been made, especially in experiment. Olurin *et al.* [2000] investigated the effects of the geometry and size of the

*Corresponding author, Tel.:+86 15334520880. E-mail address: wxz@cqu.edu.cn (Wang Xinzhu).

indenters and the density of foam on indentation responses. They extracted tearing energy of the material with a simple analysis and found it similar to the data from bearing failure, and to that of the mode I steady state fracture energy. Andrews *et al.* [2001] studied the size-dependence of the plastic strength of metal foams and found that the indentation stress varies with the diameter of the indenter. The dynamic indentation and penetration tests by Ramachandra *et al.* [2003] and Li *et al.* [2005] showed that the indentation resistance increases significantly if the velocity of indentation is greater than 10 m/s.

Tania [2012] and Xie [2013] suggested the methods of predicting the deformation and fracture behavior of sandwich panels with foam cores when subjected to quasi-static indentation. Sudheer *et al.* [2003] investigated experimentally the deep indentation response of a closed-cell Al foam at different rates of penetration. Numerical simulations and experiment were also performed for the quasi-static indentation of polymeric foams by several authors [Flores-Johnson and Li, 1995; Briody *et al.* ,2012].

The main purpose of this research is to characterize with experiment the resistance of metal foams of different relative densities against the indentation with different diameter of indenter and boundary conditions, and to measure tearing energies. A FE model is used to simulate the indentation response of metal foam subjected to flat-end cylindrical indenter, and the result is compared with experiment.

2. Material and Experimental Setup

A kind of commercially available closed-cell Al foam is adopted, which is processed with a direct foaming technique that uses TiH2 powders as an additive to the molten metal for foaming. The average cell size of the form is around 2 mm and cell wall thickness of the foam ranges from 80 to 100 μm. The typical photograph the foam is shown in Fig. 1, where it can be found that the cell size are not quite uniform, but there is overall an uniform morphology [Simone, 1998].

The indentation tests are performed on three foams with relative densities of 9%, 20% and 29%, respectively. The material testing system, INSTRAN-5569, is used for the experiment with flat-end circular cylindrical indenters (with the diameters $D = 12.7, 16, 20$ and 25.4 mm respectively). The experiment is displacement-controlled at a speed of 1 mm/min, the load and the displacement are recorded. The maximum indentation depth is about 8 mm. The specimens are supported with a rigid foundation, so the overall bending is limited. Five samples are used for each testing condition. To minimize the effects of friction, the indenters are lubricated with PTFE spray.

In order to obtain reliable testing data, the diameter of the indenter, D, should be much lager than the cell size, $d(D/d > 7$ is required in this work). The edge effect can be avoided if the indenter is at least one indenter diameter away from the edge of the plate. The size of the rectangular samples is $100 \times 100 \times 15\,\text{mm}^3$. Figure 2 shows the setup of the indentation testing.

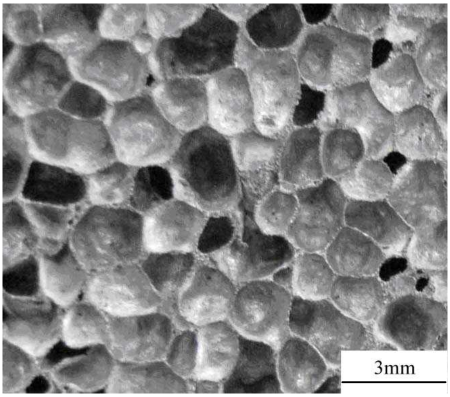

Fig. 1. Photograph of the closed-cell Al foam used.

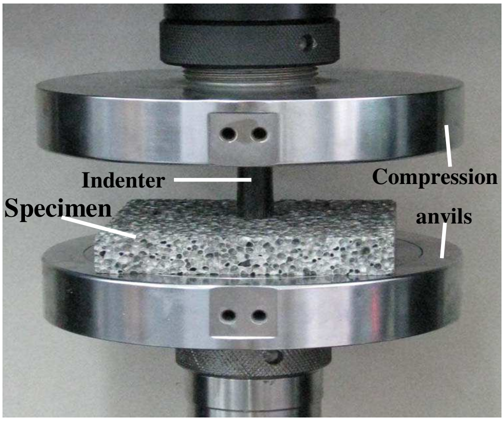

Fig. 2. Indentation test setup of Al foam.

3. Finite Element Model

Due to the practical limitations, the displacement and contact stress distribution can not be measured so that, the numerical methods is therefore employed for the simulation of the indentation process.

A numerical model mimicking the geometry, loading and boundary conditions of the indentation test is developed with the software MSC/Marc. Only a quarter of the foam plate is adopted for FE analysis due to the symmetry, as shown in Fig. 3. The solid and shell elements are adopted the mesh around the indenter is refined to improve the accuracy. The contact zone is also defined between the indenter and the sample surface, where the refined mesh is adopted. The indenter is modeled as rigid surface, which cannot overlap with the foam. The diameter of the indenter is 12.7 mm. The model contains 10080 elements in total. Since the Al foams are treated

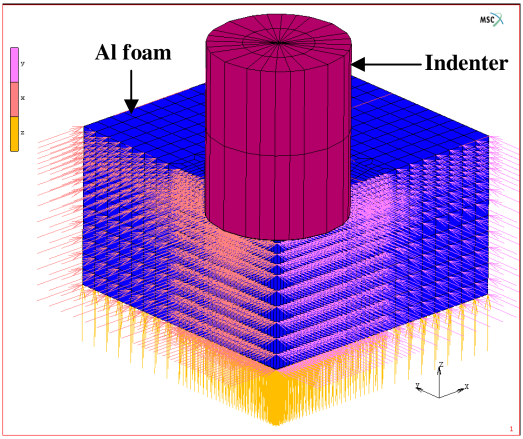

Fig. 3. FE model of Al foam under flat-end cylindrical indenter.

either as a continuum in FE model, they are assumed to behave as a homogeneous bulk material, the parameters of which correspond to the average parameters of the foam: Young's modulus $E = 2.74\,\text{GPa}$, and Poisson's ratio $\nu = 0.33$. The contact between indenter and specimen is assumed to be frictionless [Olurin *et al.*, 2000]. The bottom surface keeps fixed in the loading direction, and symmetry boundary conditions are applied to the cut faces of the quadrant while the other surfaces remain unconstrained.

Sensitivity tests are performed on the effect of mesh size, boundary conditions, and frictional condition, to ensure the FE model to be accurate with an optimum requirement on computational resources. The self-adaptive mesh control in MSC/Marc is used to reduce the effect of mesh distortion.

4. Results and Discussion

4.1. *Experiments*

4.1.1. *Characterization of Indentation*

The total force on the indenter is the sum of that to crush the foam beneath the indenter and that required to tear it at the edges of the indenter, that is

$$P = P_{\text{crushing}} + P_{\text{tearing}} = S\sigma_{pl}^{*} + 2\pi a\gamma \tag{1}$$

where P is the total load, a is the radius of indenter and S is the contact area of between the indenter and the foam, σ_{pl}^{*} is the compressive plateau stress of the foam and γ is its tearing energy.

Typical load-displacement curves (P-h curves) of the indentation of the Al foam samples of relative density $\bar{\rho} = 9\%$ with different radii of the flat-end cylindrical indenters are shown in Fig. 4, and the P-h curves of the indentation of the Al foam

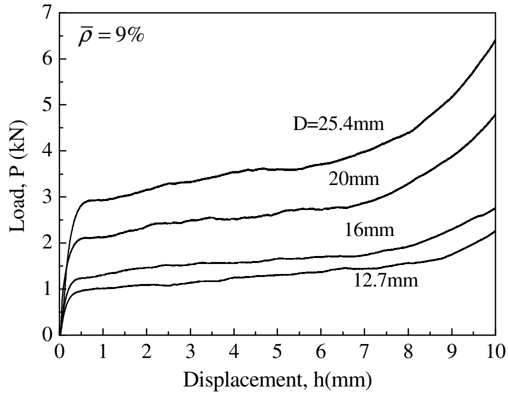

Fig. 4. *P-h* curves of indentation with different diameter of flat-end cylindrical indenters.

samples of relative densities $\bar{\rho} = 9\%, 15\%$ and 21% with the flat-end cylindrical indenter of diameter $R = 12.7$ mm are shown in Fig. 5, respectively. It can be seen that *P-h* curves are generally non-linear, due to the elastic–plastic property of the Al foam. The indentation *P-h* response of the Al foam is similar to that in the case of uniaxial compression (see Olurin, 2000; Olurin *et al.*, 2000]). At the beginning of the testing, when the indentation load is low, the *P-h* response is linear. It continues until plastic deformation (crushing of the metal foam) is triggered. After that, P approaches a plateau value, prior to an increase in stress when there is an interaction with the back face of the plate. The oscillations in the load-displacement response are due to local yield, collapse and densification (see Fig. 4). However, marked differences between uniaxial compression and indentation *P-h* data should be noted, which can be related to the nature of plastic response. The *P-h* curve in uniaxial compression appears to be independent of h within the plastic collapse regime,

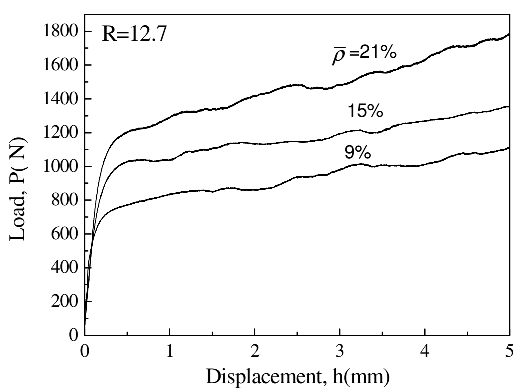

Fig. 5. indentation *P-h* curves of foam of different relative densities with flat-end cylindrical indenter.

the force required for the indenter to penetrate gradually but definitely with the increase of h. Two factors contribute to this response. Firstly, as the deformation proceeds, an increasingly larger crushed zone beneath the indenter will provide the resistance against its further penetration, which results in a steeper P-h curve, compared with the monotonic compression P-h curve. Secondly, the tearing resistance at the indenter perimeter increases with increasing h, contributing to the gradual increase in P.

In general, the contact load increases with the increase of indenter diameter, which can be understood from the fact that the increase of the indenter diameter will increase the contact area at the same indentation depth. The contact load also increases with the increase of the relative density, which is determined by the properties of the material, such as the elastic modulus, yield strength and shear modulus, which are strongly dependent on the relative density Gibson and Ashby [1997].

The above mentioned samples for indentation test are supported with a rigid foundation. In addition, the indentation response of the Al foam under simply supported boundary conditions is studied. Metal blocks are placed at the bottom of the samples to simulate the simply supported boundary conditions. The experiment results are shown in Figs. 6 and 7.

It can be seen in Fig. 6 that the boundary condition less affects the P-h curve before the load drops, which can be attributed to that the overall bending occurs to the Al foam plate subjected to the simple support boundary condition, which can not take place in the case of rigid foundation.

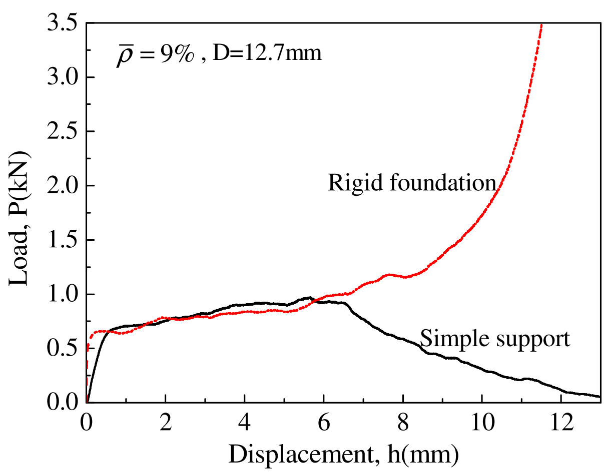

Fig. 6. P-h curves of indentation with flat-end cylindrical indenter and different boundary conditions.

Fig. 7. Photograph of the back region of the sample tested with simple support boundary condition and FEP indentation with depth 6 mm.

When the indentation depth reaches a critical value, the indentation load corresponding to rigid boundary condition increases sharply, attributed to the densification of the foam material under the indenter. There is also an obvious turning point in the indentation *P-h* curve of the Al foam with simple support boundary condition, where the load has a rapidly sudden drop. This is because the back of Al foam corresponding to indenter is free of traction, and the part of the deformation of Al foam contributed to the overall bending when the indentation depth reaches a critical value. Within a certain range of indentation depth, e.g., $h = 6\,\text{mm}$, the difference between the result with rigid foundation and that with simple support boundary condition can be ignored. It can be seen clearly in Fig. 7 that many cracks appears in the back region of the Al foam sample tested with the simple support boundary condition.

4.1.2. *Deformation Mechanism*

In order to study the deformation mechanism of Al foam, the indentation deformation zone of Al foam is cut along the longitudinal axis with an electrical discharge method, and the morphology of indentation deformation zone is photographed with an Olympus SZX12 microscope and shown in Fig. 8.

It can be seen in Fig. 8 that plastic deformation in the Al foam is localized in the region just underneath the indenter and has very little lateral spreading, because metallic foams are plastically compressible with near zero plastic Poisson's ratio [Shaw and Sata, 1966; Rinde, 1970; Timoshenko and Goodier, 1951]. The deformation is extensive within the zone of plasticity in which cells are crushed whereas, the material is in pristine condition outside it. However, the deformation during indentation is not entirely confined to the region of the compacted zone

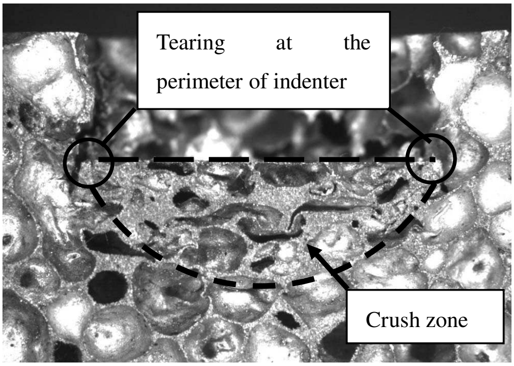

Fig. 8. Cross-sectional morphology of Al foam after indentation.

beneath the indenter; buckling can also occur to cells located somewhere farther away from the indentation location.

Furthermore, Fig. 8 reveals that the shape of the deformation zone is similar to that of porous rock [Leite and Ferland, 2001] and is approximately a spherical cap. Observations on the surface of the cylindrical cavity created by the indenter indicate a clean tearing with no bending or shear deformation of the cells.

4.1.3. *Mechanical Properties and Energy Absorption Characteristics*

Mechanical properties and energy absorption characteristics of metallic foams can also be investigated with indentation test. Indentation tests have been used to measure the properties of engineering materials for more than a century. The indentation testing technique most commonly used is hardness test. An important advantage of this technique lies in the fact that it requires a relatively small volume of material, thus enabling repeated testing on relatively smaller specimens.

Mechanical properties obtained from indentation test are the hardness (H), tearing energy (γ) and shear strength (τ^*). H is defined as

$$H = \frac{P}{A} \tag{2}$$

where P is the applied load and A is the projected contact area of indentation. For flat-end cylindrical indenter, the projected contact area is $A = \pi a^2$. Rearranging Eq. (1) gives

$$\gamma = \frac{P - S\sigma_{pl}^*}{2\pi a} = \frac{P - \pi a^2 \sigma_{pl}^*}{2\pi a} = \frac{(\bar{p} - \sigma_{pl}^*)a}{2} \tag{3}$$

where $\bar{p}$ is the total indentation pressure. The relationship between the tearing energy and the shear strength is Gill *et al.* [1980]

$$\tau^* = \frac{\gamma}{d} \tag{4}$$

where d is the diameter of foam cell.

The energy absorption capability, w, and the energy absorption efficiency, η, are the two important parameters to evaluate the energy absorption characteristics of Al foam. w, the absorbed energy per unit volume in a certain strain interval $[\varepsilon_1, \varepsilon_2]$ is equal to the area below the stress-strain curve and can be expressed as

$$w = \int_{\varepsilon_1}^{\varepsilon_2} \sigma(\varepsilon) d\varepsilon \tag{5}$$

η is defined as the ratio of energy absorbed by an ideal energy absorber to that absorbed by the actual foam

$$\eta = \frac{\int_{\varepsilon_1}^{\varepsilon_2} \sigma(\varepsilon) d\varepsilon}{\sigma_0(\varepsilon_2 - \varepsilon_1)} \tag{6}$$

H, γ, w and η are calculated using the P-h curves of Al foam with different sizes of indenters, relative densities of the foams, and the same indentation depth, $h_c = 6$ mm, as shown in Figs. 9–12.

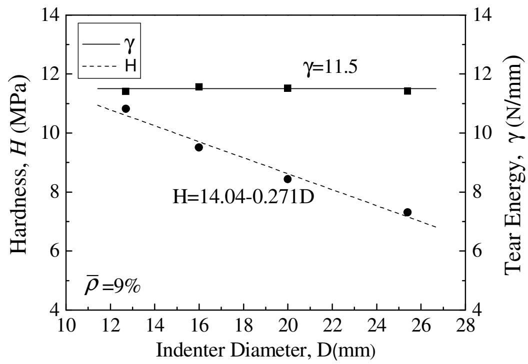

Fig. 9. H-D and γ-D curves of Al foam.

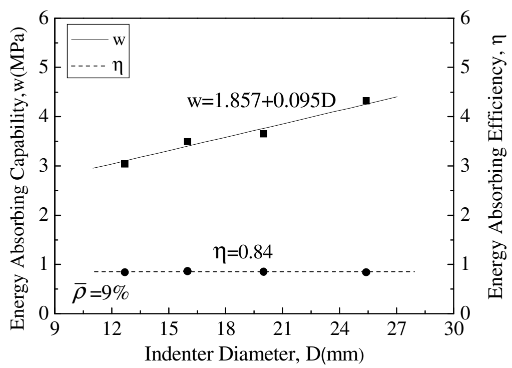

Fig. 10. w-D and η-Dcurves of Al foam.

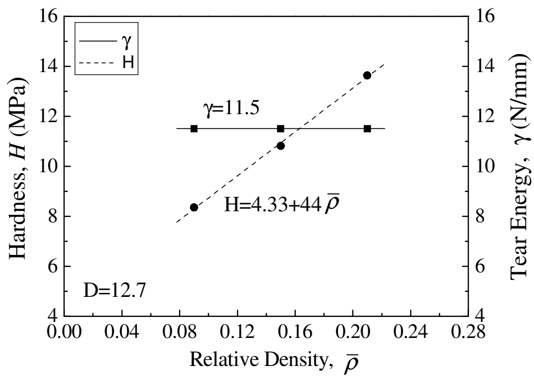

Fig. 11. H-$\bar{\rho}$ and γ-$\bar{\rho}$ curves of Al foam.

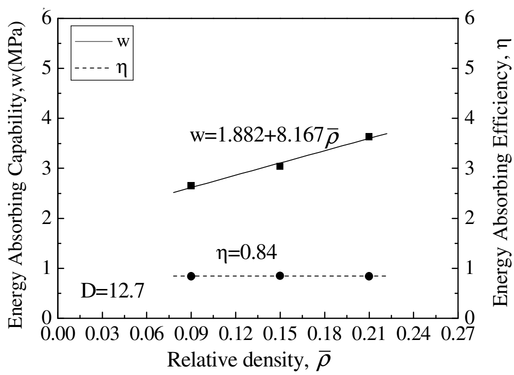

Fig. 12. w-$\bar{\rho}$ and η-$\bar{\rho}$ curves of Al foam.

It can be seen in Figs. 9–12 that the hardness decreases linearly with the increase of the indenter size and increases linearly with the increase of relative density of the foams. Energy absorption capability of the Al foam increases linearly with the increase of the indenter size or the relative density of Al foams. The tearing energy density and energy absorption efficiency are independent of indenter sizes and relative density of Al foams, and the average values are 11.5 N/mm and 0.84, respectively.

4.2. *FE Analysis*

Figure 13 shows the contour maps of the displacement in the Al foam subjected to indentation, which is obtained with FE simulation. The variations of the displacement components in different directions are shown in Fig. 14.

As shown in Figs. 13 and 14, the maximum deformation appears in the contact region and the displacement decreases gradually with the increase of the distance from the indentation center and approaches approximately zero when the distance approaches the diameter of the indenter. If the indentation depth is very small, the foam cells contacting the indenter edges are not torn. The indentation load is born by a larger area of the Al foam sample, and the scope of the displacement

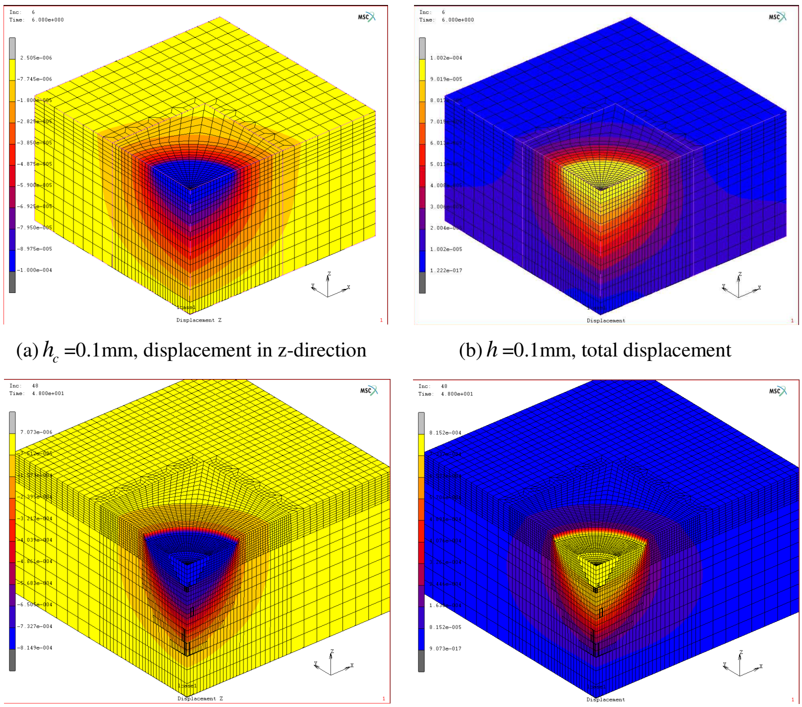

(a) h_c =0.1mm, displacement in z-direction (b) h =0.1mm, total displacement

(c) h =0.8mm, displacement in z-direction (d) h =0.8mm, total displacement

Fig. 13. Contour maps of displacement.

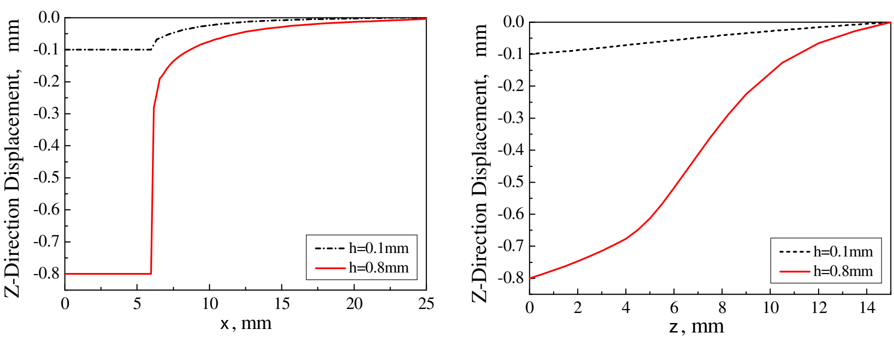

Fig. 14. Displacement distributions in x-direction and z-direction.

field is larger. The deformation is confined to the material directly beneath the indenter with very little lateral spread as the indenter reaches a certain depth. The indentation deformation in the Al foam sample is non-uniform.

The transition of displacement is located at the contact edge of the foam. The foam cells contacting the edge of indenter appear to sink, but the phenomenon is not detected in the indentation test with the conventional methods. The boundary of the densified foam is hemispherical, which agrees with the phenomenon observed in the indentation test.

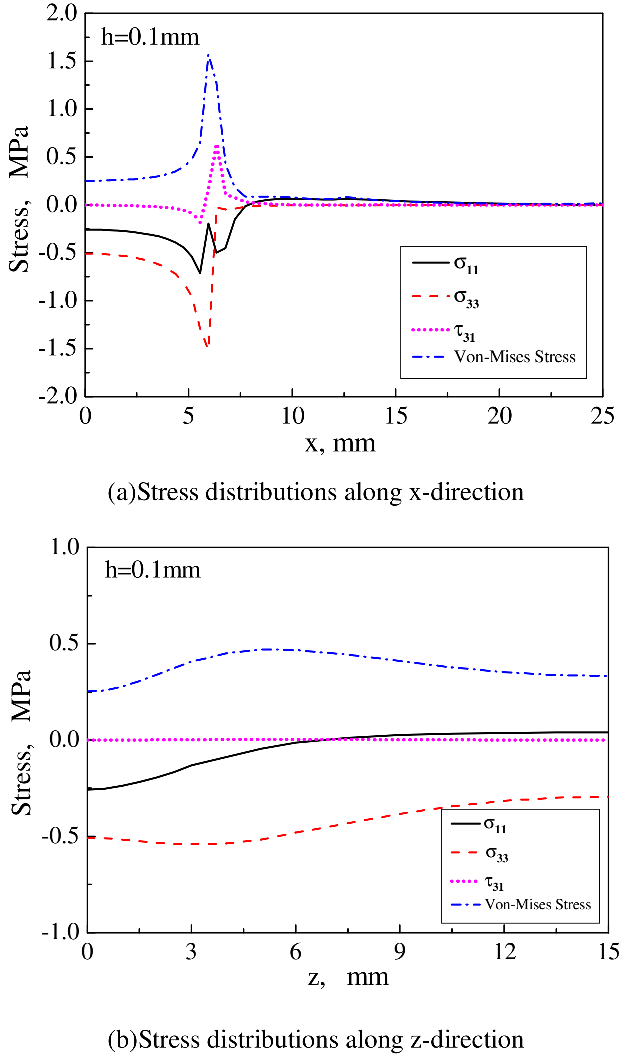

Fig. 15. Stress distributions in x-direction and z-direction when $h = 0.1\,\text{mm}$.

Plastic deformation of the foam can be modeled with Von-Mises yield criterion. Figs. 15 and 16 show the distributions of normal stresses (σ_{11}, σ_{33}), shear stress (τ_{31}), equivalent plastic strain and Von-Mises stress obtained with the FE simulation. It can be seen that stress concentration occurs in the contact zone, which results from torsion of the foam cells contacting the indenter edges. The stress distributes mainly in the region of the size of indenter diameter, and the normal stress in the region corresponds to indenter's end, and shear stress in the region corresponds to the edges of the contact zone. When the indentation depth is smaller,

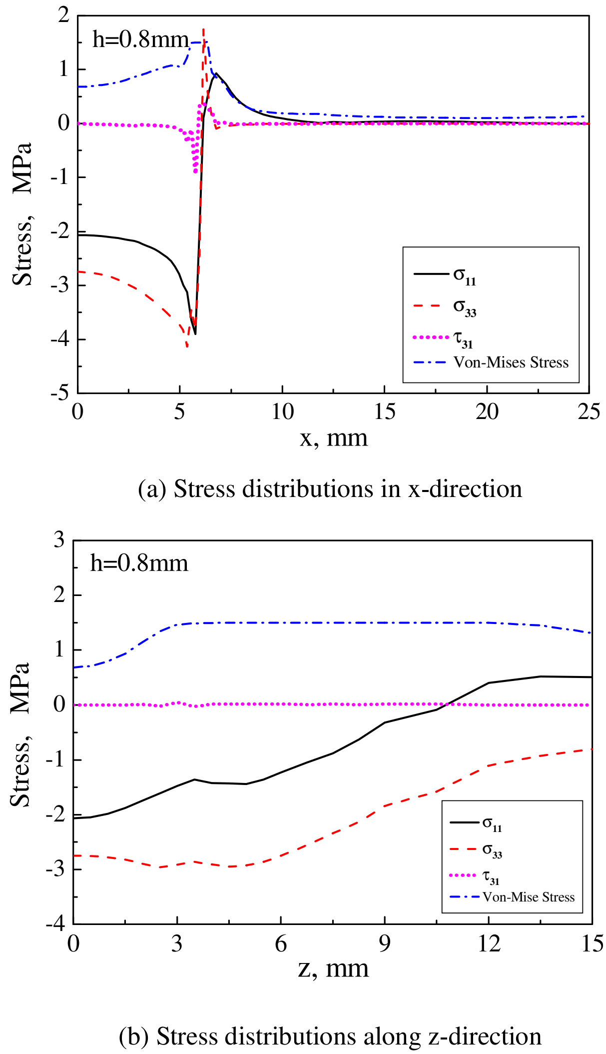

Fig. 16. Stress distributions in x-direction and in z-direction as $h = 0.8\,\text{mm}$.

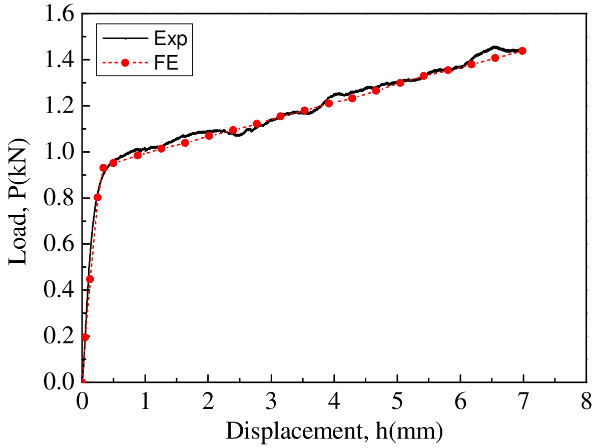

Fig. 17. Comparison between the experimental FE simulated *P*-*h* curves.

the normal stress components σ_{11} and σ_{33} are positive and have a certain gradient outward from the indentation center.

When the indentation depth is larger, the absolute value of the corresponding stress is also larger, and effect of the rigid foundation on the Al foam is obvious. Normal stress component σ_{33} is dominant, but shear stress component τ_{31} is also significant. Because the foam cells at the edges of contact zone are torn, the normal and shear stress components change from negative values to positive ones as the indentation depth reaches a critical value. Shear stress component at the indentation center is always zero regardless of the depth of indentation, indicating that the state of stress in this region should be pure compression.

As the Von-Mises stress at the edge of contact zone reaches the yield strength of the Al foam, plastic deformation may inevitably take place in this region. Figure 17 shows the comparison between the indentation curve obtained with FE simulation and that obtained in experiment, provided the same indenter size and relative density, where satisfactory agreement can be found and the insignificant difference might be attributed to that the friction between the indenter and the foam sample is not taken into account in FE simulation.

5. Conclusions

In this article the indentation of a kind of Al foam with flat-end cylindrical indenter was investigated with both finite element simulation and experiment. A set of indentation tests were conducted to investigate the effect of the size of the indenter, the relative density of the foam sample and the boundary condition on the hardness, energy absorption capability and energy absorption efficiency of the Al foam. The main results are summarized as follows:

1) The indentation curve of the Al foam under the flat-end cylindrical indenter is similar to that in uniaxial compression, but there are some differences, indicating different deformation mechanism.
2) The experiment results show that the compacted zone is restricted to the region directly under the indenter and the lateral spreading is insignificant. The tearing of the foam cells occurs in the vicinity of the densified region. Both the experiment and the simulation reveal that the shape of the deformation zone is hemispherical, which is similar to that of porous rock.
3) The mechanical properties of the Al foam, such as tearing energy (γ) and shear strength (τ^*), can be obtained with the indentation test. It was found that the hardness decreases linearly with the increasing of indenter size and increases linearly with the increase of relative density of the foam. The energy absorption capability of the Al foam increases linearly with the increase of the indenter size or the relative density of the foam. The tearing energy and energy absorption efficiency are independent of the indenter size and the relative density of the Al foam.
4) At a certain range of indentation depth, the difference between the *P*-*h* curve obtained with the rigid foundation condition and that obtained with simple support condition can be ignored.
5) The FE simulation reveals that the transition of displacement is located at the edge of contact zone. The foam cells contacting the edge sink, but the phenomenon can not be detected in the indentation test with the conventional methods. Stress concentration occurs in the contact zone. The stress distribute mainly in the region corresponding to one indenter diameter, the normal stress components distribute mainly in the region corresponding to the indenter's end, and the shear stress components distribute mainly in the region corresponding to the edge of the contact zone.

Acknowledgments

The authors are grateful acknowledge the financial support from the Fundamental Research Funds for the Central Universities under grant No. CDJRC10240002, CDJZR12240067, CDJZR12110072, and China Postdoctoral Science Foundation (No. 2011M500067).

References

Gibson, L. J. and Ashby, M. F. [1997]. Cellular Solids: Structure and Properties, 2nd edition. Cambridge University Press, Cambridge, UK.

Ashby, M. F., Evans, A. G., Fleck, N. A., Gibson, L. J., Hutchinson, J. W., and Wadley, H. N. G. [2000]. Metal Foams: A Design Guide, Butterworth Heinemann.

Olurin, O. B., Fleck, F. A., and Ashby, M. F. [2000] "Indentation resistance of an aluminium foam," *Scripta Materialia* **43**(11), 983–989.

Andrews, E. W., Gioux, G., Onck, P., and Gibson, L. J. [2001] "Size effects in ductile celluar solids Part II: experimental results," *Int. J. Mechanical Sciences* **43**, 701–713.
Ramachandra, S., Sudheer, P., and Ramamurty, U. [2003] "Impact energy absorption in an Al foam at low velocities," *Scripta Materialia* **49**(8), 741–745.
Li, Q. M., Maharaj, R. N., and Reid, S. R. [2005] "Penetration resistance of aluminium foam," *Int. J. Vehicle Design.* **37**(2/3), 175–183.
Vodenitcharova, T., Kabir, K., and Hoffman, M. [2012] "Indentation of metallic foam core sandwich panels with soft aluminium face sheets," *Materials Science & Engineering A* **558**, 175–185.
Xie, Z., Zheng Z., and Yu, J. [2013] "Localized indentation of sandwich panels with metallic foam core, Analytical models for two types of indenters," *Composites: Part B.* **31**, 212–217.
Sudheer, Kumar P., Ramachandra, S., and Ramamurty, U. [2003] "Effect of displacement-rate on the indentation behavior of an aluminum foam," *Materials Science and Engineering A* **347**, 330–337.
Flores-Johnson, E. A. and Li Q. M. [2010] "Indentation into polymeric foams," *International Journal of Solids and Structures* **47** 1987–1995.
Briody, C., Duignan, B., Jerrams, S., and Tiernan, J. [2012] "The implementation of a visco-hyperelastic numerical material model for simulating the behaviour of polymer foam materials," *Computational Materials Science* **4**, 231–245.
Simone, A. E. and Gibson, L. J. [1998] "Effects of solid distribution on the stiffness and strength of metallic foams," *Acta Mat.* **46**, 3109–3150.
Olurin, O. B. [2000], *Deformation and Fracture of Cellular Foams*, Ph.D. Thesis, Cambridge University Engineering Department.
Olurin, O. B., Fleck, N. A., Ashby, M. F. [2000], *Mater Sci. Eng. A.* **291**, 136–146.
Shaw, M. C. and Sata, T. [1966] "The plastic behavior of cellular materials," *J. Mech. Sci.* **8**(7), 469–472.
Rinde, J. A. [1970] "Poisson's ratio for rigid plastic foams," *Appl. Polymer Sci.* **14**, 1913–1926.
Timoshenko, S. and Goodier, J. N. [1951], *Theory of Elasticity* McGraw-Hill, New York.
Leite, M. H. and Ferland, F. [2001] "Determination of unconfined compressive strength and Young's modulus of porous materials by indentation tests," *Eng. Geology.* **59**, 267–280.
Gill, D. E., Pichette, C., and Rochon, P. *et al.* [1980] "Relation between some of the methods for predicting the penetration rate of full-face boring machines." In: Proceedings of the 13^{th} Canadian Symposium Rock Mechanics, CIM Sp. **22**, 1103–1110.